光学学报

基于Pt/GaN/AlGaN异质结高响应度双波段紫外探测器

吴刚[1,2,3]，唐利斌[1,2,3*]，郝群[1**]，邓功荣[2***]，张逸韵[4]，秦强[2]，袁绶章[2]，王静宇[2]，魏红[2]，严顺英[2]，谭英[2]，孔金丞[2]

[1]北京理工大学光电学院，北京 100081；
[2]昆明物理研究所，云南 昆明 650223；
[3]云南省先进光电子材料与器件重点实验室，云南 昆明 650223；
[4]中国科学院半导体研究所固体照明研究开发中心，北京 100090

摘要 提出一种在AlGaN基PIN器件的p-GaN表面上沉积Pt，形成肖特基势垒(SB)-PIN异质结器件，器件的能带和载流子的输运发生了变化，这种新型光电探测器实现了双波段紫外探测，可分别工作在光伏和光电导模式下。器件在275 nm波长的紫外光照射的负偏置电压下，工作模式为光伏探测，当入射光功率密度为100 μW/cm^2，偏置电压为−10 V时，器件得到最大响应度(0.12 A/W)；当偏置电压为−0.5 V时，器件得到最大探测率(1.0×10^{13} cm·Hz$^{1/2}$·W^{-1})。器件在正偏置电压工作模式下可作为高响应、高增益的光电导探测器，当偏置电压为+10 V时，用275 nm和365 nm波长的紫外光照射(光功率密度为100 μW/cm^2)，器件的响应度分别为10 A/W和14 A/W，外量子效率分别为4500%和4890%。所设计的双波段多功能器件将极大地扩展基于AlGaN的紫外探测器的用途。

关键词 探测器；双波段紫外探测器；AlGaN；异质结；响应度

中图分类号 O472 **文献标志码** A **DOI：** 10.3788/AOS221312

1 引　言

日盲紫外(UV)探测器因其在精确制导、导弹预警、航天器追踪、明火监控、生物成像、紫外保密通信等应用领域的巨大潜力而备受关注[1-3]。AlGaN三元化合物半导体材料可通过调整Ga和Al的成分，可使其带隙在3.4 eV(GaN)到6.2 eV(AlN)之间变化，具有覆盖波长≤365 nm的宽带紫外光探测能力。同时，由于GaN/AlGaN材料的异质结构在AlGaN和GaN界面上具有高浓度二维电子气，材料载流子具有较高的浓度和迁移率[4]，利用AlGaN材料制备的紫外探测器比其他宽禁带材料(SiC、CsTe)紫外探测器具有更高的探测灵敏度[5]，因此AlGaN材料是制备日盲紫外探测器的理想材料之一。目前，利用高浓度的二维电子气来提高载流子收集效率的肖特基势垒探测器(SBD)[6-7]和金属-半导体-金属(MSM)探测器[8-9]、利用器件内建电场来提高载流子收集效率的PIN光电二极管[10-11]和雪崩光电二极管(APD)[12-13]是最常用的研究器件，均能获得较优的性能。

在复杂的目标环境和短距离非视距光通信系统中，灵敏度高且工作频谱宽的探测器有助于提高探测器的适应性[14-15]，目前，科研人员报道了一些关于双波段紫外光电探测器的研究，但针对日盲波段的研究仍然有限。

本文将功函数为5.36 eV的金属Pt沉积到GaN/AlGaN材料上表面功函数为7.5 eV的p-GaN层表面，不进行退火，形成肖特基接触，以取代AlGaN基PIN器件传统的Ni/Au、Ti/Pt/Au等多层金属并经高温退火形成欧姆接触[16-17]，p-GaN材料在与Pt接触的一侧形成能带向下弯曲的肖特基势垒，与AlGaN材料本身的PIN结构结合，形成SB-PIN异质结结构，使器件的能带、内建电场和载流子输运机制与PIN和SBD器件相比发生变化，从而产生新的器件工作机制和光电特性，器件可探测日盲紫外和可见盲紫外双波段。同时，通过调整施加在器件上的偏置电压，使器件能用作高速光电二极管或具有高增益的光电导体。

2 实　验

本实验中，AlGaN基PIN异质结材料采用MOCVD生长，在蓝宝石衬底上依次生长1000 nm厚的AlN层、1000 nm厚的应变超晶格层、500 nm厚的n型$Al_{0.6}Ga_{0.4}N$窗口层、100 nm厚重掺杂n$^+$-$Al_{0.55}Ga_{0.45}N$

收稿日期：2022-06-14；**修回日期**：2022-07-25；**录用日期**：2022-08-12；**网络首发日期**：2022-08-22

基金项目：国家重点研究开发计划(2019YFB2203404)、云南省创新团队项目(2018HC020)

通信作者：*sscitang@163.com；**qhao@bit.edu.cn；***gongrong.deng@hotmail.com

电极接触层、230 nm 厚的本征 $Al_{0.48}Ga_{0.52}N$ 吸收层、30 nm 厚的 p 型 $Al_{0.48}Ga_{0.52}N$ 和 150 nm 厚的 p 型 GaN 重掺电极接触层，其结构和参数如图 1(a)所示。图 1(b)所示为用轮廓仪测试表面形貌的结果，在 210 μm×210 μm 的面积内，材料的表面粗糙度约为 5 nm。

为了分析本实验制备器件和传统 PIN 器件的区别，用同一 AlGaN 材料分别制作 Pt/p-GaN/AlGaN 异质结器件(SB-PIN 器件)和传统 PIN 器件。SB-PIN 器件的制备过程为：首先，清洗材料，通过光刻和反应离子刻蚀(RIE)形成直径为 700 μm 的器件台面，通过电子束蒸发在 n^+-AlGaN 层上沉积多层 Ti/Al/Ni/Au 金属，并在 550 ℃、N_2 气氛下快速退火形成欧姆接触的下电极；然后生长 SiO_2/SiN_x 复合介质膜钝化器件侧壁和下台面 n^+-AlGaN 表面，以减少表面漏电；最后，使用光刻、刻蚀工艺打开上台面窗口之后，将 Pt 沉积到 p-GaN 层表面以形成 SB-PIN 结构的器件。PIN 器件则是在上述制备过程中，当下电极制备完成后，在上台面的 p-GaN 表面沉积多层 Ni/Au/Ni/Au 金属，经 850 ℃、O_2 气氛下快速退火后形成欧姆接触的上电极，然后经过钝化膜生长和电极开孔后完成器件制备。

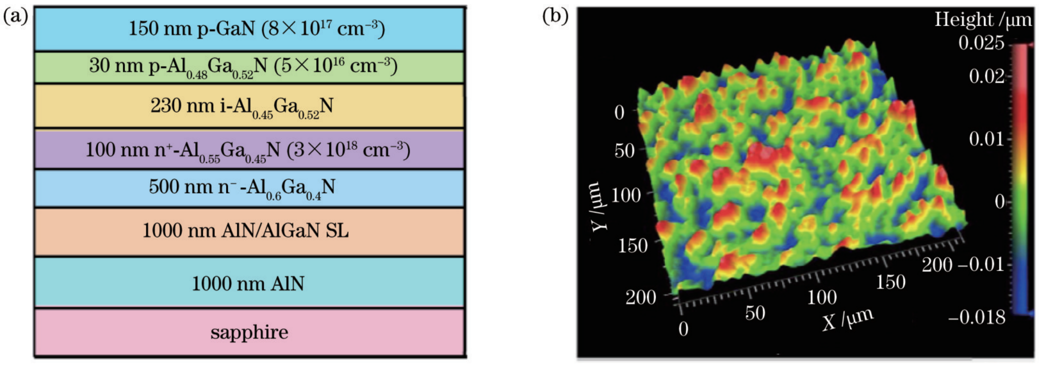

图 1　材料结构及表征。(a)外延薄膜结构示意图；(b)通过轮廓仪测量的表面形貌

Fig. 1　Material structure and characterization. (a) Schematic of epitaxial film structure; (b) surface topography measured by profilometry

本研究采用紫外光功率计标定发射波长分别为 275 nm 和 365 nm 的商用紫外 LED 光源，用 Keithley 2400 数字源表检测探测器的电流信号。在响应速度测试中，LED 光源由外部电源调制，探测器的实时电流响应由示波器读取。

3　实验结果与讨论

图 2(a)所示为室温下，在功率密度为 100.9 μW/cm²、波长为 275 nm 的紫外光照射下 SB-PIN 和 PIN 器件的电流密度(J)随电压(V)的变化曲线，可以看到，SB-PIN 器件的暗电流和光电流均比 PIN 器件小，当暗电流在负偏置电压(−10～0 V)和正偏置电压(+1.7～+10 V)范围内，SB-PIN 器件的暗电流比 PIN 器件小了一个数量级，并且随着偏置电压的增加，SB-PIN 器件与 PIN 器件的暗电流比值逐渐增大。SB-PIN 器件的光电流在−10～+1.8 V 的偏置电压范围内比 PIN 器件小了近 66.7%。与 PIN 器件不同的是，SB-PIN 器件在正偏置电压(+2.5～+10 V)范围内，其光电流比暗电流大，并且随偏置电压的增加其变化越来越大，当偏置电压为+10 V 时，光电流与暗电流的比值高达 15。图 2(b)所示为室温下，功率密度为 100.9 μW/cm²、波长为 365 nm 的紫外光照射下 SB-PIN 器件的光电流和暗电流变化曲线，其光电流在负偏置电压(−10～0 V)范围内比暗电流稍大，与 275 nm 光照射下相同的是，SB-PIN 器件在正偏置电压(+2.5～+10 V)范围内，其光电流比暗电流大，并且随偏置电压的增加其变化越来越大，当偏置电压为+10 V 时，光电流是暗电流的 10 余倍。

图 2(c)、(d)所示分别为 SB-PIN 器件在 275 nm 和 365 nm 光照射下的响应度和探测率的测量结果，响应度、探测率结果由器件的 J-V 结果计算而来，响应度(R_i)的计算公式为

$$R_i = \frac{I_{ph} - I_d}{p}, \tag{1}$$

探测率(D^*)的计算公式为

$$D^* = R_i \sqrt{\frac{A}{2qI_d}}, \tag{2}$$

式中：I_{ph} 为器件的光生电流；I_d 为器件的暗电流；A 为器件的面积；p 为入射光功率；q 为单位电子的电荷量。275 nm 光照射下，SB-PIN 器件在偏置电压为−10 V 时，响应度最大值为 0.12 A/W，外量子效率超过 50%；当偏置电压为−0.5 V 时，探测率达到 1×10^{13} cm·Hz$^{1/2}$·W^{-1}；当偏置电压为+10 V 时，响应度最大值为 10 A/W，外量子效率超过 4500%，探测率达到 5×10^{10} cm·Hz$^{1/2}$·W^{-1}。365 nm 光照射下，SB-PIN 器件在偏置电压为+10 V 时，响应度最大值为 14.4 A/W，外量子效率超过 4800%，探测率达到 8×10^{10} cm·Hz$^{1/2}$·W^{-1}。图 2(c)、(d)中分别标注了在 275 nm 和 365 nm 光照射，且外量子效率 $\eta=1$ 的理想情况下，光电二极管响应度(R)的理论极限和对应的

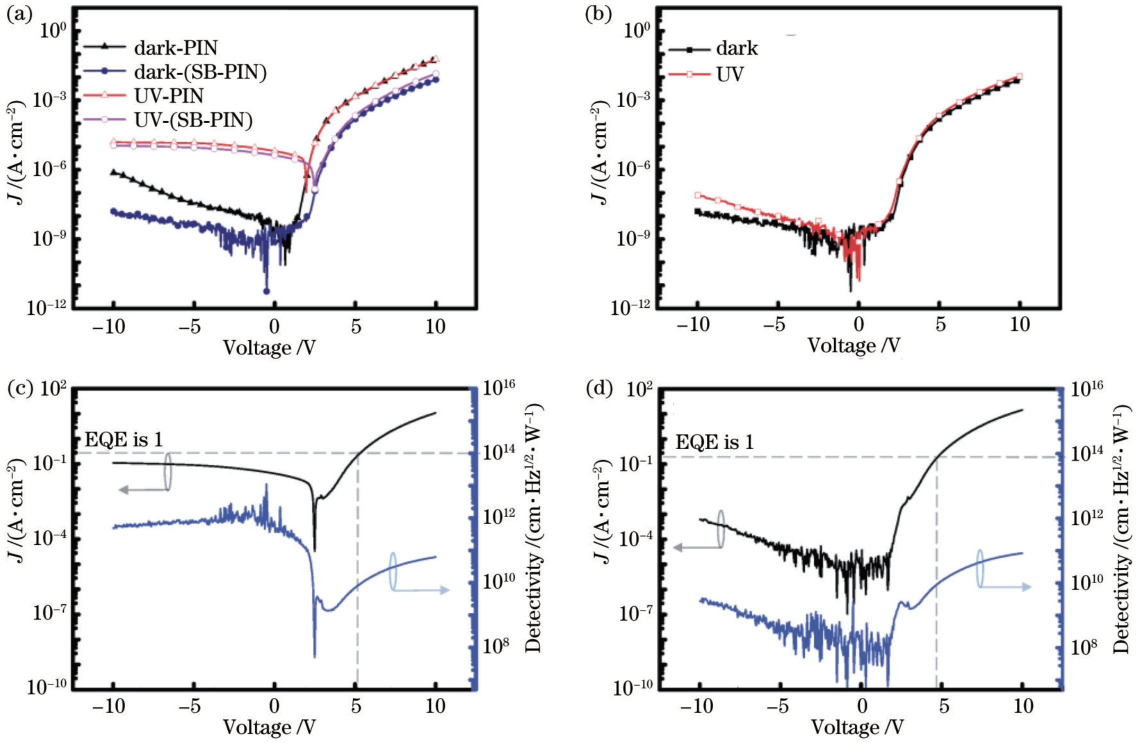

图 2 器件在功率密度为 100 μW/cm^{2}的紫外光照射下的光电特性。(a) SB-PIN、PIN 器件的暗电流密度和在 275 nm 光照射下的光电流密度;(b) SB-PIN 器件的暗电流密度和在 365 nm 光照射下的光电流密度;(c) SB-PIN 器件在 275 nm 光照射下的响应度和探测率;(d) SB-PIN 器件在 365 nm 光照射下的响应度和探测率

Fig. 2 Photoelectric characteristics of the device under UV irradiation with an incident optical power of 100 μW/cm^2. (a) Dark current density and photocurrent density of SB-PIN and PIN photodetectors with 275 nm illumination; (b) dark current density and photocurrent density of SB-PIN photodetector with 365 nm illumination; (c) responsivity and detectivity of SB-PIN device with 275 nm illumination; (d) responsivity and detectivity of SB-PIN device with 365 nm illumination

偏置电压。R的理论极限计算公式为

$$R=\frac{q\eta}{h\upsilon}\approx\frac{\eta\lambda}{1.24},\tag{3}$$

式中:h为普朗克常数;υ为频率,单位为 Hz;λ为入射光束的波长,单位为 μm。在 275 nm 和 365 nm 光照射下,光电二极管器件R的理论极限值分别为 0.22 A/W 和 0.29 A/W,对应的偏置电压分别为 +5.1 V 和 +4.9 V。由图 2 可知,当偏置电压高于 +5.1 V(275 nm)和 +4.9 V(365 nm)时,SB-PIN 器件有高于光电二极管理论极限的响应度,因此该器件此时工作在与光电二极管不同的工作机制下。

为进一步研究器件在不同偏置电压下的工作机制,测试了 SB-PIN 器件的光响应度随入射光功率变化的规律。图 3(a)、(b)所示分别为具有不同功率的 275 nm 和 365 nm 紫外光入射时,SB-PIN 器件响应度随偏置电压的变化曲线。图 3(c)所示为当 275 nm 紫外光入射,偏置电压分别为 −10 V 和 +10 V 时,SB-PIN 器件响应度随入射光功率的变化关系,结果表明,在负偏置电压下,响应度几乎不随入射光功率的变化而改变,这是 PIN 光电探测器的典型特征[18-19],器件在正偏置电压下,响应度随入射光功率的增大而减小,当偏置电压为 +10 V 时,其关系为$R\propto P^{-0.781}$。图 3(d)所示为在 365 nm 紫外光入射、偏置电压为正的情况下,SB-PIN 器件的响应度随入射光功率的变化规律,其规律与 275 nm 紫外光入射,偏置电压为正时基本一致,响应度随入射光功率的增大而减小,当偏置电压为 +10 V 时,其关系为$R\propto P^{-0.787}$。器件在正偏置电压下,响应度随入射光功率的增大而减小,符合光导型器件的特征,这也解释了器件在正偏置电压大于 5 V 时具有高的响应度和外量子效率。

图 4 所示为 SB-PIN 器件的响应时间测试结果。从图 4(a)可以看到,在 275 nm 的光照射下,偏置电压为 −10 V 时,响应时间较短(τ_{rise}=190 μs),当偏置电压为 +10 V 时,器件的响应时间为τ_{rise}=2.0 ms。从图 4(b)可以看到,器件在 365 nm 紫外光照射下,偏置电压为 +10 V 时响应时间τ_{rise}=2.3 ms,这与近年来报道的 GaN/AlGaN 紫外探测器响应时间[20]相近。

本研究将功函数为 5.36 eV 的金属 Pt 沉积到功函数为 7.5 eV 的 p-GaN 窗口层表面上,根据金属-半导体接触理论,p-GaN 与 Pt 接触的一侧形成能带向下弯曲的肖特基势垒,与材料的 PIN 结构结合,器件形成 SB-PIN 异质结结构,其工作模式发生了变化。当偏置电压为负值时,PIN 势垒较大,外电场压降主要出现在 PIN 势垒区,表面肖特基结处有较小的压降,而外电场与肖

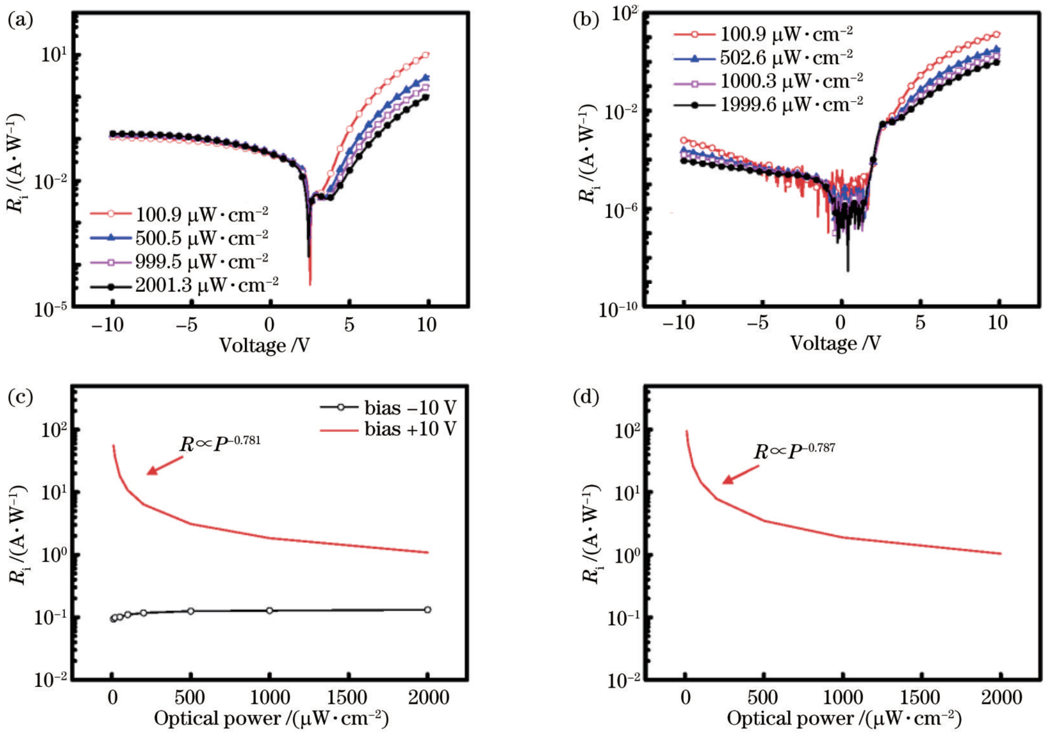

图 3　响应度随偏置电压和入射光功率密度的变化关系。(a)在不同功率密度的 275 nm 光照射下，响应度随偏置电压的变化关系；(b)在不同功率密度的 365 nm 光照射下，响应度随偏置电压的变化关系；(c) 275 nm 光照下，偏置电压为－10 V、＋10 V 时，响应度随入射光功率密度的变化结果；(d)在 365 nm 光照射下，偏置电压为＋10 V 时响应度随入射光功率密度的变化结果

Fig. 3　Responsivity changed with bias voltage and optical power density. (a) Responsivity changed with bias voltage under 275 nm illumination with different power densities; (b) responsivity changed with bias voltage under 365 nm illumination with different power densities; (c) responsivity changed with incident light power density at bias voltage of －10 V and ＋10 V under 275 nm illumination; (d) responsivity changed with incident light power density at bias voltage of ＋10 V under 365 nm illumination

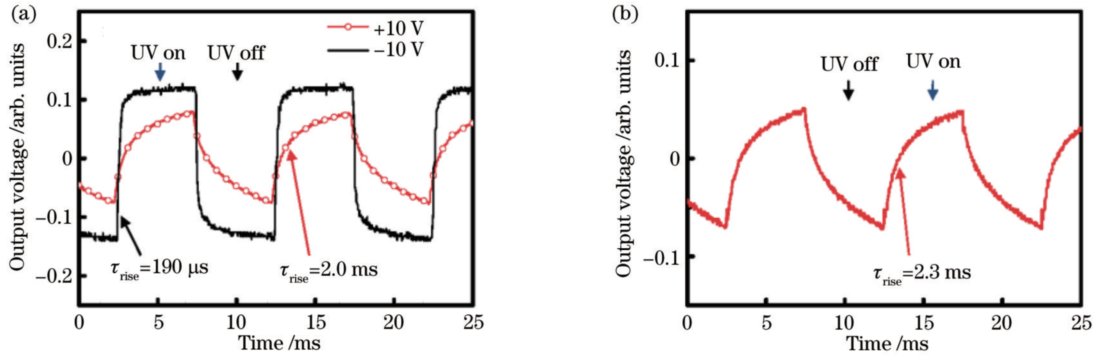

图 4　器件的响应时间测试结果。(a)在 275 nm 光照射下，偏置电压为－10 V 和＋10 V 时的测试结果；(b)在 365 nm 光照射下，偏置电压为＋10 V 时的测试结果

Fig. 4　Temporal response test results of the photodetector. (a) Test results at the bias voltage of －10 V and ＋10 V under 275 nm illumination; (b) test result at the bias voltage of ＋10 V under 365 nm illumination

特基结的电场方向相反，导致肖特基势垒减弱，275 nm 光照射时，被减弱的肖特基势垒对 PIN 结产生的光生载流子的阻挡作用减弱，其响应度仅比传统 PIN 器件稍小，量子效率也能大于 50%。365 nm 紫外光照射时，被减弱的肖特基势垒对光生载流子的收集和传输作用减弱；同时，GaN 和 AlGaN 之间的势垒 ΔE 也阻挡了光生载流子的收集和传输，因此 365 nm 波长紫外光照射时光响应很小，如图 5(a)所示。当偏置电压为正值时，肖特基结的内建电场与外电场方向一致，p-GaN 与 Pt 接触一侧的能带弯曲变大，同时，PIN 势垒区由于受到正向偏置电压作用，其势垒减小，使得器件整体的内建电场变小，光生载流子的传输和收集受到外电场控制，光电转换行为变为光电导模式，从而产生了较大的响应度和外量子效率，其工作原理如图 5(b)所示。

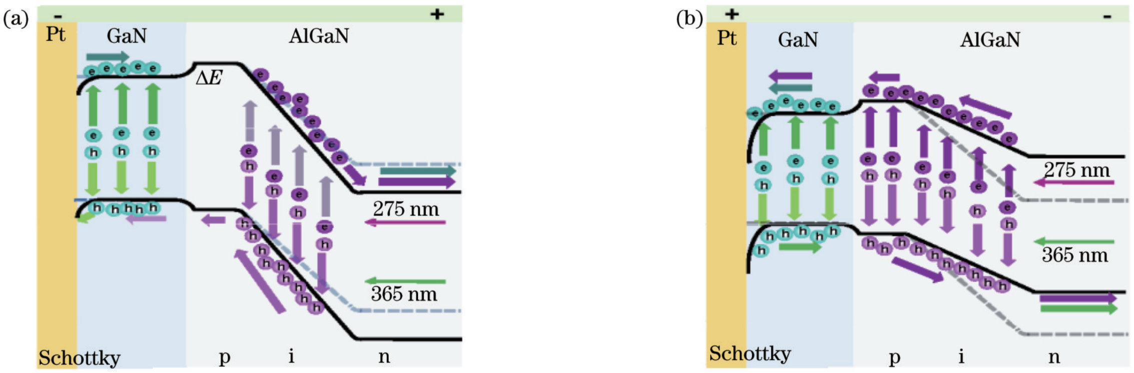

图 5　器件的能带图和工作原理。(a)负偏置电压时;(b)正偏置电压时

Fig. 5　Energy band diagrams and working principles of the device. (a) Under negative bias voltage; (b) under positive bias voltage

4　结　　论

提出一种 Pt/p-GaN/AlGaN 异质结紫外光电探测器,可实现日盲紫外和可见盲紫外双波段探测,并且可通过调整施加在器件上的偏置电压,实现器件工作模式在光伏和光电导之间切换。在负偏置电压、275 nm 光照射下,探测器作为高速的日盲紫外光伏探测器工作,具有略小于 PIN 结构紫外探测器的响应度和探测率;在高正偏置电压下,探测器作为高灵敏度、高增益的日盲和可见盲紫外光电导探测器,使得所提出的紫外光电探测器在双波段、高速和高增益应用方面都具有良好的前景。

参　考　文　献

[1] Razeghi M, Rogalski A. Semiconductor ultraviolet detectors[J]. Journal of Applied Physics, 1996, 79(10): 7433-7473.

[2] Xu Z Y, Ding H P, Sadler B M, et al. Analytical performance study of solar blind non-line-of-sight ultraviolet short-range communication links[J]. Optics Letters, 2008, 33(16): 1860-1862.

[3] 刘火平, 尹达一, 张荣杰, 等. 地面紫外探测高空高速再入目标分析与验证[J]. 光学学报, 2017, 37(12): 1211004.
Liu H P, Yin D Y, Zhang R J, et al. Feasibility analysis and verification of high speed reentry target on ground ultraviolet detection[J]. Acta Optica Sinica, 2017, 37(12): 1211004.

[4] Jang H W, Jeon C M, Kim K H, et al. Mechanism of two-dimensional electron gas formation in Al$_x$Ga$_{1-x}$N/GaN heterostructures[J]. Applied Physics Letters, 2002, 81(7): 1249-1251.

[5] 蒋科. AlGaN 材料类同质外延生长及日盲紫外探测器研究[D]. 长春:中国科学院长春光学精密机械与物理研究所, 2019.
Jiang K. Study on the AlGaN quasi-homoepit axial growth and solar-blind UV detectors[D]. Changchun: Changchun Institute of Optics, Fine Mechanics and Physics, Chinese Academy of Sciences, 2019.

[6] Katz O, Garber V, Meyler B, et al. Gain mechanism in GaN Schottky ultraviolet detectors[J]. Applied Physics Letters, 2001, 79(10): 1417-1419.

[7] Liang F Z, Feng M X, Huang Y N, et al. AlGaN-based Schottky barrier deep ultraviolet photodetector grown on Si substrate[J]. Optics Express, 2020, 28(12): 17188-17195.

[8] Tang X, Ji F W, Wang H, et al. Temperature enhanced responsivity and speed in an AlGaN/GaN metal-heterostructure-metal photodetector[J]. Applied Physics Letters, 2021, 119(1): 013503.

[9] Brendel M, Helbling M, Knauer A, et al. Top- and bottom-illumination of solar-blind AlGaN metal-semiconductor-metal photodetectors[J]. Physica Status Solidi A, 2015, 212(5): 1021-1028.

[10] Monroy E, Hamilton M, Walker D, et al. High-quality visible-blind AlGaN p-i-n photodiodes[J]. Applied Physics Letters, 1999, 74(8): 1171-1173.

[11] Cicek E, McClintock R, Cho C Y, et al. Al$_x$Ga$_{1-x}$N-based back-illuminated solar-blind photodetectors with external quantum efficiency of 89%[J]. Applied Physics Letters, 2013, 103(19): 191108.

[12] Reddy P, Breckenridge M H, Guo Q, et al. High gain, large area, and solar blind avalanche photodiodes based on Al-rich AlGaN grown on AlN substrates[J]. Applied Physics Letters, 2020, 116(8): 081101.

[13] Gautam L, Jaud A G, Lee J, et al. Geiger-mode operation of AlGaN avalanche photodiodes at 255 nm[J]. IEEE Journal of Quantum Electronics, 2021, 57(2): 4500106.

[14] Lü Q F, Jiang H X, Lau K M. High gain and high ultraviolet/visible rejection ratio photodetectors using p-GaN/AlGaN/GaN heterostructures grown on Si[J]. Applied Physics Letters, 2020, 117(7): 071101.

[15] Pandit B, Schubert E F, Cho J. Dual-functional ultraviolet photodetector with graphene electrodes on AlGaN/GaN heterostructure[J]. Scientific Reports, 2020, 10: 22059.

[16] Ho J K, Jong C S, Chiu C C, et al. Low-resistance ohmic contacts to p-type GaN[J]. Applied Physics Letters, 1999, 74(9): 1275-1277.

[17] Zhou L, Lanford W, Ping A T, et al. Low resistance Ti/Pt/Au ohmic contacts to p-type GaN[J]. Applied Physics Letters, 2000, 76(23): 3451-3453.

[18] Arulkumaran S, Ng G I, Vicknesh S. Enhanced breakdown voltage with high Johnson's figure-of-merit in 0.3-μm T-gate AlGaN/GaN HEMTs on silicon by (NH$_4$)$_2$S$_x$ treatment[J]. IEEE Electron Device Letters, 2013, 34(11): 1364-1366.

[19] Endoh A, Yamashita Y, Hirose N, et al. High performance AlGaN/GaN metal-insulator-semiconductor high electron mobility transistors fabricated using SiN/SiO$_2$/SiN triple-layer insulators[J]. Japanese Journal of Applied Physics, 2006, 45(4B): 3364-3367.

[20] Tian H J, Liu Q L, Zhou C X, et al. Hybrid graphene/GaN ultraviolet photo-transistors with high responsivity and speed[J]. Applied Physics Letters, 2018, 113: 121109.

Dual-Band and High-Responsivity Ultraviolet Detector Based on Pt/GaN/AlGaN Heterojunction

Wu Gang[1,2,3], Tang Libin[1,2,3*], Hao Qun[1**], Deng Gongrong[2***], Zhang Yiyun[4], Qin Qiang[2], Yuan Shouzhang[2], Wang Jingyu[2], Wei Hong[2], Yan Shunying[2], Tan Ying[2], Kong Jincheng[2]

[1] *School of Optics and Photonics, Beijing Institute of Technology, Beijing* 100081, *China*;

[2] *Kunming Institute of Physics, Kunming* 650223, *Yunnan, China*;

[3] *Yunnan Key Laboratory of Advanced Photoelectronic Materials & Devices, Kunming* 650223, *Yunnan, China*;

[4] *Research and Development Center for Solid-State Lighting, Institute of Semiconductors, Chinese Academy of Sciences, Beijing* 100090, *China*

Abstract

Objective Solar blind ultraviolet (UV) detectors based on AlGaN ternary compound semiconductors have attracted much attention due to their great application potential in fields such as precision guidance, missile warning, spacecraft tracking, open flame monitoring, bioimaging, and UV secure communication. In increasingly complex target environments and short-range non-line-of-sight optical communication systems, UV detectors with high sensitivity and wide working bandwidth are required. At the same time, new material structure designs and device structure research make the UV detectors have higher performance and wider application. In this work, metal Pt with a work function of 5.36 eV is deposited on the surface of a p-GaN layer with a work function of 7.5 eV on the upper surface of GaN/AlGaN material without annealing. The Schottky contact is formed to replace the Ohmic contact formed by the traditional deposition of Ni/Au, Ti/Pt/Au, and other multilayer metals in an AlGaN-based PIN device and annealed at a high temperature. The p-GaN material forms a Schottky barrier with an energy band bending downward on the side contacting with Pt and combined with the PIN structure of the AlGaN material itself. An SB-PIN heterojunction structure is formed in the device, which changes the energy band, the built-in electric field, and the carrier transport mechanism of the device compared with PIN and SBD devices and results in a new operating mechanism and photoelectric characteristics of the device. The device has a high responsivity under a positive bias voltage and realizes dual-band detection (275 nm and 365 nm).

Methods The fabrication process of the device proposed in this work is as follows: After the wafer cleaning, a device mesa with a diameter of 700 μm is defined by reactive ion etching (RIE). Ti/Al/Ni/Au metal layers are deposited on the n^+-AlGaN layer by an e-beam evaporator, and the sample is then annealed at 550 ℃ to form an ohmic contact. Then, SiO_2/SiN_x composite dielectric film is grown to passivate the side wall of the device and the n^+-AlGaN surface of the lower mesa surface to reduce surface leakage. After the window in the upper mesa surface is opened by lithography and etching process, Pt is deposited on the surface of the p-GaN layer to form a device with an SB-PIN structure. In order to compare the differences between the device prepared in this work and the traditional PIN device, a traditional PIN device is simultaneously fabricated with the same AlGaN material. The PIN device is prepared by depositing multiple layers of Ni/Au/Ni/Au metal on the p-GaN surface of the upper mesa surface after a lower electrode is prepared, and then an Ohmic contact upper electrode is developed after rapid annealing at 850 ℃ in O_2 atmosphere. Finally, the device is prepared after passivation film growth and electrode opening.

Results and Discussions The dark current and photocurrent of the SB-PIN device are both smaller than that of the PIN device under a UV light (275 nm) with a power density of 100.9 $\mu W/cm^2$. Under a bias voltage of −10 V, the maximum responsivity is 0.12 A/W, and the external quantum efficiency is more than 50%. Different from the PIN device, in a positive bias voltage (+2.5 V–+10 V), the photocurrent of the SB-PIN device is larger than the dark current, and as the bias voltage increases, the change is more and more obvious. Under a bias voltage of +10 V, the photocurrent to dark current ratio is up to 15 times, and the maximum responsivity is 10 A/W. The external quantum efficiency is over 4500%, and the detectivity reaches up to 5×10^{10} $cm\cdot Hz^{1/2}\cdot W^{-1}$. Due to the existence of the Schottky barrier on the surface, the SB-PIN device also responds to a UV light of 365 nm. Under a 365 nm LED with a power density of 100.9 $\mu W/cm^2$ and a bias voltage of +10 V, the maximum responsivity is 14.4 A/W, and the external quantum efficiency is more than 4800%. The detectivity reaches 8×10^{10} $cm\cdot Hz^{1/2}\cdot W^{-1}$ (Fig. 2). By exploring the relationship between the responsivity and bias voltage and the incident optical power (Fig. 3), it is explained that the operating mechanism of the SB-PIN device is photoconductive under a positive bias voltage (≥5 V) and a UV light of 275 nm and 365 nm, respectively. The response speed τ_{rise} equals 2.0 ms (275 nm) and 2.3 ms (365 nm), respectively (Fig. 4). Under a UV light of 275 nm and a negative bias voltage, the operating mechanism is photovoltaic, and the response speed τ_{rise} equals 190 μs (Fig. 4).

Conclusions The UV photodetector based on Pt/p-GAN/AlGaN heterojunction proposed in this paper can realize dual-band (solar blind UV and visible blind UV) detection, and the device can be switched between photovoltaic and photoconductive modes by adjusting the bias voltage. In negative bias voltage, the PIN barrier becomes stronger, and the external voltage drop mainly acts on the PIN depletion region. The surface Schottky junction is smaller. As the direction of the external electric field and the Schottky junction electric field is opposite, the Schottky junction which reduces the resistance of photon-generated carriers under a light of 275 nm is weakened. The device has a responsivity and detectivity that are slightly smaller than those of the PIN structure detector, which can be used as a high-speed solar blind UV photovoltaic detector. Under a high positive bias voltage, the direction of the Schottky junction built-in electric field and the external electric field is the same, and the band bending of p-GaN contacting with Pt is stronger. At the same time, the PIN depletion region is narrowed, which makes the overall built-in electric field of the device smaller andlets transmission and collection of photon-generated carriers controlled by the external electric field. As a result, the device operating mechanism is changed to the photoconductive mode, and the detector operates as a high-sensitivity, high-gain, solar-blind, and vision-blind UV photoconductive detector, which makes the proposed UV photodetector more promising for dual-band, high-speed, and high-gain applications.

Key words detectors; dual-band ultraviolet detectors; AlGaN; heterojunction; responsivity